

# Analysis of coastal lee waves along the coast of Texas observed in advanced very high resolution radiometer images

Xiaofeng Li,<sup>1</sup> Quanan Zheng,<sup>2</sup> William G. Pichel,<sup>1</sup> Xiao-Hai Yan,<sup>2</sup> W. Timothy Liu,<sup>3</sup> and Pablo Clemente-Colón<sup>1</sup>

**Abstract.** We examine a group of wave-like cloud patterns that occurred along the coast of Texas on a National Oceanic and Atmospheric Administration satellite advanced very high resolution radiometer IR images taken on January 22, 1999. These wave-like cloud patterns were interpreted to be signatures of a coastal lee wave packet on the basis of simultaneous field observations and theories developed by *Zheng et al.* [1998a]. The wave packet contains 13 waves with crest lines generally parallel to the coastline. The lengths of leading wave crest lines are longer than 500 km. The average wavelength is 9.5 km, ranging from 6.2 to 14.7 km. The width of the horizontal distribution band of the wave packet is as wide as 113 km. This case represents the most energetic coastal lee wave packet that has ever been reported.

## 1. Introduction

The coastal lee wave is a small-scale atmospheric gravity wave occurring along the lee side of a coast as defined by *Zheng et al.* [1998a]. Formally, these waves are analogous to mountain lee waves [e.g., *Gjevik and Marthinsen*, 1978] and lee waves induced by isolated islands [e.g., *Mitchell et al.*, 1990; *Vachon et al.*, 1994; *Li et al.*, 1998a]. Lee waves are frequently imaged by the visible and IR channels of advanced very high resolution radiometer (AVHRR) onboard the National Oceanic and Atmospheric Administration (NOAA) series of Polar-orbiting Operational Environmental Satellites (POES) as wave-like cloud patterns [*Gjevik and Marthinsen*, 1978; *Mitchell et al.*, 1990]. Over the ocean, wind speed fluctuations at the sea surface associated with the lee waves modulate the sea surface roughness, and thus lee waves can also be imaged by synthetic aperture radar (SAR) through the resonant or Bragg scattering mechanism. By analyzing the wave-like patterns on SAR images, information on lee wave dynamics can be retrieved [*Vachon et al.*, 1994; *Zheng et al.*, 1998a].

The first reported case of coastal lee wave observation with SAR is an ERS-1 SAR image along the western coast of Taiwan Strait [*Zheng et al.*, 1998a]. The waves occurred as wave packets containing 6–17 waves and were characterized by crest lines that were generally parallel to the coastline with crest lengths ranging from 20 to 80 km and wavelengths ranging from 1.7 to 4.2 km with an average of 3 km. It was verified by a physical model that the land-sea breeze circulation driven by the land-sea temperature difference [*Simpson*, 1994] was an important coastal lee wave generation mechanism.

A similar case of atmospheric wave packets was reported in

an offshore area near the Pakistani coast from space shuttle photographs taken on April 29, 1993 [*Zheng et al.*, 1998b]. The packet contained 19 waves, with an average wavelength of 1 km and a crest line longer than 250 km. The packet had highly nonlinear characteristics and was categorized in the morning glory family, as observed previously in northern Australia [*Clarke*, 1972; *Smith*, 1988]. The land breeze and katabatic flow were believed to be possible generation mechanisms.

In this paper we will provide new evidence concerning the genesis of coastal lee waves. The wave patterns were seen in NOAA satellite AVHRR IR images of January 22, 1999. Simultaneously observed surface boundary conditions reveal that a land breeze circulation existed at the imaging time. The scales of the waves indicate that this wave packet is more energetic than coastal lee waves cases reported previously.

## 2. Observations

### 2.1. Interpretation of NOAA AVHRR Images

The data used for this study consists of NOAA CoastWatch [*Li et al.*, 1998b] AVHRR channel 4 (11  $\mu\text{m}$ ) images taken from the NOAA 14 and NOAA 15 POES satellites. POES satellites operate operationally in a pair to ensure that the data, for any region of the Earth, are no more than 6 hours old. CoastWatch is a NOAA program managed by National Environmental Satellite Data and Informational Service (NESDIS) with CoastWatch Regional Nodes located at NOAA laboratories and offices in eight coastal states. Input data for the production of CoastWatch imagery are high-resolution picture transmission (HRPT) level 1b data sets. These consist of AVHRR detector output from the five channels of the AVHRR with appended calibration and Earth location information. For the U.S. east coast, Great Lakes, and Gulf of Mexico regions, data sets are received from every satellite pass over the Wallops Station, Virginia, reception mask. Satellite data from Wallops are transmitted to the NESDIS Central Environmental Satellite Computer System (CEMSCS) in Suitland, Maryland, as soon as each satellite overpass is completed. Processing into level 1b products proceeds automatically as soon as the complete pass has been received, followed by CoastWatch mapping over each region covered by the satellite

<sup>1</sup>National Oceanic and Atmospheric Administration/National Environmental Satellite Data and Information Service, Camp Springs, Maryland.

<sup>2</sup>College of Marine Studies, University of Delaware, Newark, Delaware.

<sup>3</sup>Jet Propulsion Laboratory, California Institute of Technology, Pasadena, California.

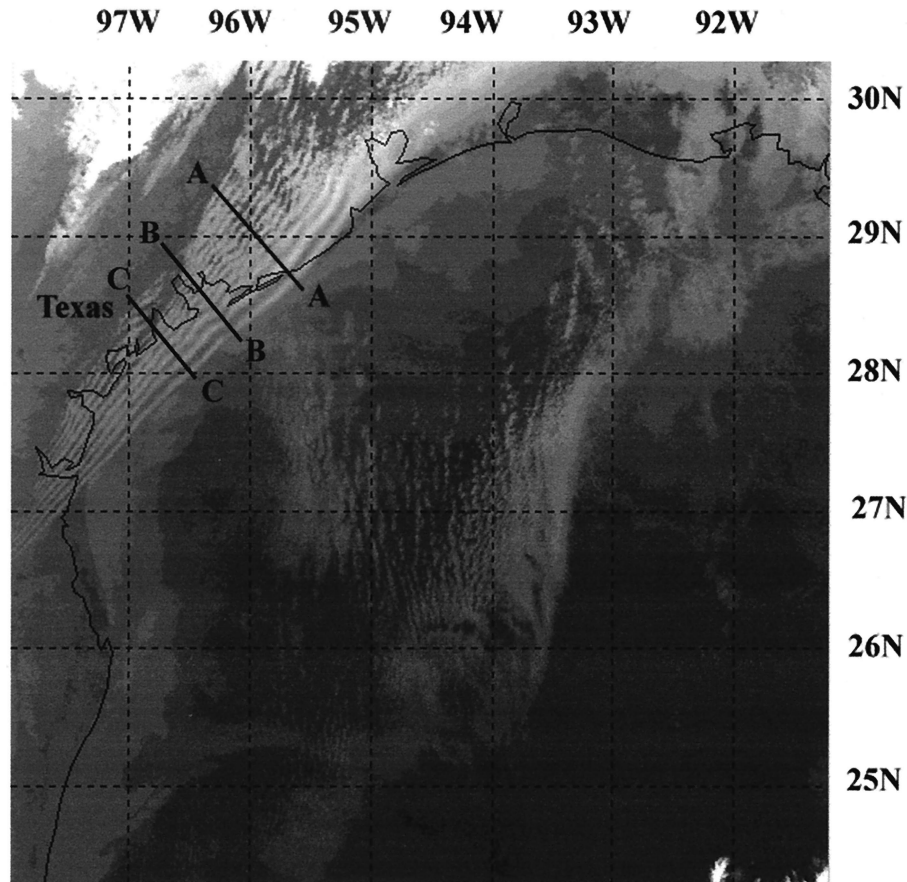


**Figure 1a.** NOAA-14 AVHRR IR image of the northwestern Gulf of Mexico and adjacent coastal regions received at 0933 UT (coded 0933) on January 22, 1999. Image resolution is  $\sim 1.3$  km. Alternative dark-bright cloud patterns along the coast are interpreted to be signatures of coastal lee waves.

pass. All five AVHRR channels (visible channels 1 and 2 at 0.6 and 0.9  $\mu\text{m}$ , short-wavelength IR channel 3 at 3.7  $\mu\text{m}$ , and long-wavelength IR channels 4 and 5 at 11 and 12  $\mu\text{m}$ ) are mapped to a series of “sector” images from the region maps. These sector maps are  $512 \times 512$  pixels in size for selected areas within the region. Sectors are produced at near full-resolution,  $\sim 1.3$  km pixel $^{-1}$  at 30°N latitude (AVHRR full resolution is 1.1 km at nadir).

The two consecutive AVHRR IR images are shown in Figures 1a and 1b. The image shown in Figure 1a was taken at 0933 UT on January 22, 1999, by NOAA 14 satellite, and that shown in Figure 1b was taken at 1421 UT on the same day by NOAA 15. For simplicity the two images will be coded hereafter as 0933 and 1421, respectively. The images cover the area from 24°17' to 30°17'N latitude and from 91°13' to 97°58'W longitude, which includes the northwestern Gulf of Mexico, part of the Mexico, all of the Texas, and the most of the Louisiana coastal regions.

Both images are from AVHRR channel 4. Therefore the shading levels in the image represent the average brightness temperature within each resolution cell. In this case the higher temperatures are represented by darker values, and lower temperatures are represented by lighter values. The plume-like patterns in white and light shading are cloud patterns.

On image 0933 we can see that the clouds along the coast appear as alternating bright and dark bands, in a wave-like pattern. We assume that the pattern represents a packet of

atmospheric waves. The packet contains 13 waves distributed in a band with a width of 113 km. The wavelength ranges from 6.2 to 14.7 km, with an average of 9.5 km. The crest line of leading waves inside the image is as long as 532 km. After nearly 5 hours the packet cannot clearly be seen in image 1421, implying that the waves had decayed. We examined the images received prior to 0933; there were also no wave-like patterns to be found, implying that the life span of the wave packet was on the order of 5 hours. The interpretation results are shown in Figure 2.

## 2.2. Surface Boundary Conditions

### 2.2.1. Surface analysis charts.

The surface analysis weather charts produced every 6 hours by the NOAA National Centers for Environmental Prediction (NCEP) show the locations of synoptic scale high- and low-pressure centers with associated surface fronts and troughs for specific analysis times. The central pressure is depicted with three or four digits. Arrows point to the 24 hour forecast positions. The pressure analysis has a 4 mbar contour interval. In this case the surface analysis charts at 0000, 0600, 1200, and 1800 UT on January 22, 1999, which covered the duration of the observed atmospheric wave packet, are given in Figures 3a–3d. We see that for the 0000 UT chart a high surface pressure system (1028 mbar) was centered in the middle Atlantic, and a low-pressure system (995 mbar) dominated the southwest United States. The subsequent charts show that the low-pressure center

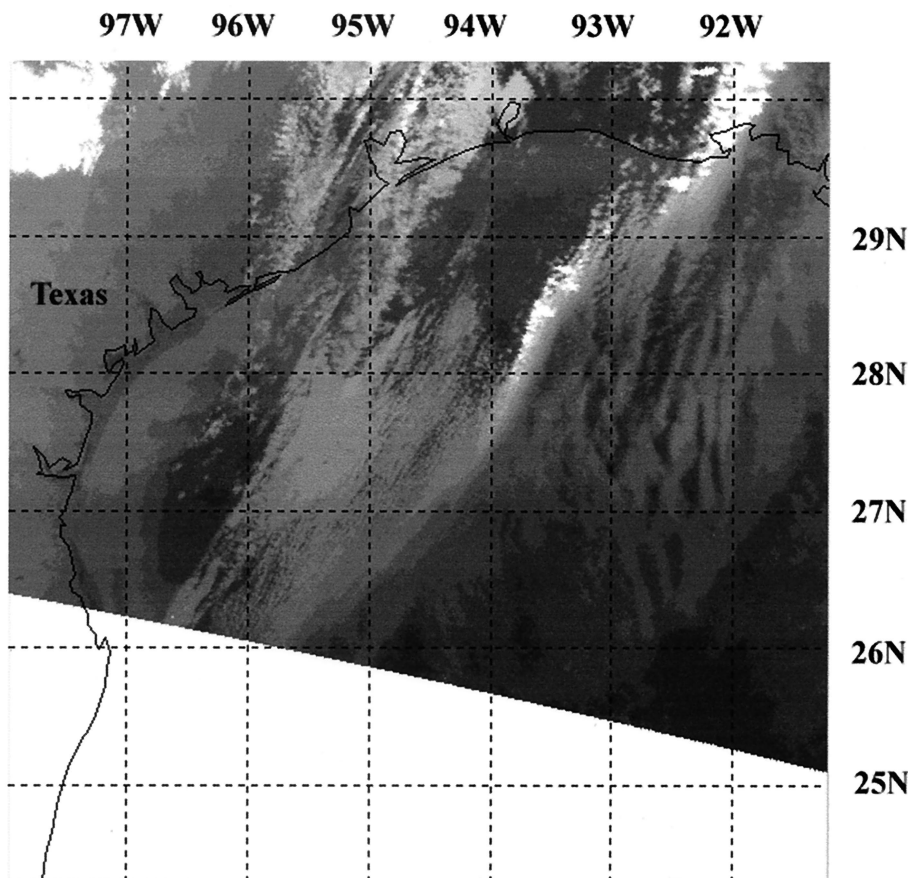


**Figure 1b.** Same as Figure 1a but received at 1421 UT (coded 1421) by the NOAA 15 satellite.

moved toward the northeast and that a high-pressure center was moving toward the south. The surface front associated with the low-pressure system moved from the continent to the western side of the Gulf of Mexico at about 1200 UT, and continued eastward until 1800 UT.

**2.2.2. Field observations.** We also obtained winds and air temperatures measured at nearby buoy stations (42020 and 42035) and Coastal-Marine Automated Network (C-MAN) stations (Port Arkansas, Texas (PTAT2), and Sabine, Texas (SRST2)). The instrument locations and sensor elevations are given in Table 1.

Hourly average air temperature time series measured at these stations are shown in Figure 4. We see that the average air temperatures measured by the buoys were about 2°–4°C higher than those measured over the land by the C-MAN stations prior to the imaging time. This rather large land-sea temperature difference is favorable for land-sea breeze circulation development [Simpson, 1994; Zheng *et al.*, 1998a].

The 10 min average wind speed and direction measured at the two C-MAN stations are shown in Figures 5a and 5b, respectively. For comparison the times of the two consecutive AVHRR images are marked with vertical lines. The first two lines represent the times of the images of Figures 1a and 1b. We see that both wind speed and direction were changing when the 0933 image was taken. At the PTAT2 station the wind speed changed from 15 to 2 m s<sup>-1</sup>, and the wind direction changed from 165° to 245° (clockwise from north) within 30 min. Over the same period, similar changes were also observed at the SRST2 station, with the wind speed dropping from 13 to

10 m s<sup>-1</sup> and direction changing from 155° to 255°. On average the wind vector changed from (14 m s<sup>-1</sup>, 160°) to (6 m s<sup>-1</sup>, 250°) during the passage of the front.

**2.2.3. Radiosonde observations.** A radiosonde is a balloon-borne instrument used to measure and transmit meteorological data simultaneously while ascending through the atmosphere. The instrument consists of sensors for the measurement of pressure, temperature, relative humidity, and velocity. The United States participates in the World Meteorological Organization's (WMO's) World Weather Watch program by maintaining and operating about 90 radiosonde stations in a network of civilian and military sites on the continental United States and its remote islands. The average continental U.S. radiosonde station separation is about 315 km, and two observations (at 0000 and 1200 Z) are scheduled daily.

The nearest radiosonde station to the study region is located at Corpus Christi, Texas (27°34.8'N, 97°13.0'W). The wave shown in Figure 1a passed this station 3 hours prior to the radiosonde deployment. The virtual and dew point temperature profiles, measured at 1200 UT on January 22, 1999, are plotted in Figure 6.

It is feasible to estimate the cloud top height by using the temperature measured by the AVHRR IR channel. In this case the cloud top temperature across the wave pattern on the AVHRR channel 4 image varies from 284.5° to 292.5°K. By comparing with the radiosonde profile we found that these temperatures correspond to the 850 mbar level, which is the bottom altitude of a strong atmospheric inversion layer. There-

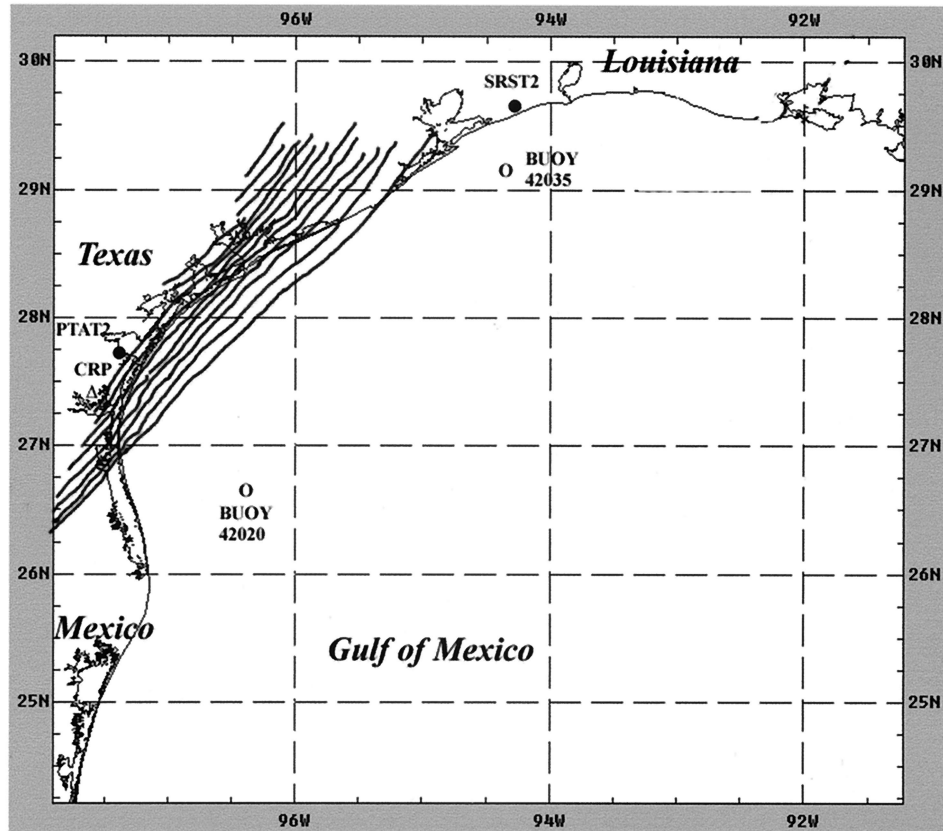


**Figure 2.** An interpretation map of Figures 1a and 1b. The coastal lee waves are shown as a group of heavy lines. Locations of Coastal-Marine Automated Network (C-MAN) stations PTAT2 and SRST2, buoy stations 42020 and 42035, and Corpus Christi, Texas, radiosonde station (CRP) are as marked.

fore it is reasonable to conclude that the wave occurred below the 850 mbar level. In addition, from Figure 6 we see that the difference between the dew point temperature and the virtual temperature,  $\Delta T$ , was small between the 970 and 850 mbar levels but increased above these levels. This indicates that clouds existed from the 970 to 850 mbar levels ( $\Delta T$  minimum). The wind between 970 and 850 mbar was uniform at 21 knots ( $10.8 \text{ m s}^{-1}$ ) from  $300^\circ$ .

### 3. Dynamical Analysis

#### 3.1. Genesis

The above data indicate that the average wavelength and crest line length of the atmospheric waves under investigation are as large as 9.5 and 500 km, respectively. Both parameters are far beyond the range of previously reported coastal lee wave cases [Zheng *et al.*, 1998a, 1998b]. The wavelength scale is close to typical mountain lee wave wavelengths of 10 km [Gossard and Hooke, 1975; Panchev, 1985]. The airflow lift caused by a mountain obstacle is a key mechanism for generating a mountain lee wave. However, given the topography, it is unreasonable to interpret these waves as mountain lee waves. Examining the geomorphologic features of the study area, we see that conditions are not favorable for generation of mountain lee waves.

The region covered by the wave-like clouds includes the coastal plain of the Gulf of Mexico. The nearest feature that is steep enough to force an upward airflow is the Balcones Escarpment, the eastern border of Edward Plateau, located

around 200 km inland from the coast. Mountain lee waves are generally stationary with respect to a mountain, i.e., they are standing. As will be discussed, physically, the observed waves may be stationary waves but with respect to the atmospheric front rather than to the land. It is reasonable therefore to conclude that the waves are not mountain lee waves.

We assume that the observed waves are coastal lee waves, although they are much stronger than the previously reported cases. The physical model developed by Zheng *et al.* [1998a] shows that the land breeze circulation, which is driven by the land-sea temperature difference, is an important mechanism for generating coastal lee waves. In our case the surface boundary conditions indicate that this is also true. The observed waves occurred in the middle latitudes (from  $27^\circ$  to  $30^\circ\text{N}$  latitude) during the local early winter. The land-sea temperature difference reaches a maximum value during this season. The measurements shown in Figure 4 reveal that the sea surface air temperature was  $2^\circ\text{--}4^\circ\text{C}$  higher than the land surface air temperature before the waves occurred, implying a favorable condition for generating the land breeze. On the other hand, the observations of wind speed and wind direction recorded at the C-MAN stations are shown in Figures 5a and 5b. We can see that the original wind vector prior to the front passage is ( $14 \text{ m s}^{-1}$ ,  $160^\circ$ ), while the wind vector after the front passage is ( $6 \text{ m s}^{-1}$  from  $250^\circ$ ). Therefore, using the vector analysis method, we can see that a wind vector of ( $15 \text{ m s}^{-1}$  from  $319^\circ$ ) existed during the front passage. Compared with the map, we see that this wind vector is oriented across the coastline. This indicates that a land breeze circulation with a wind speed of  $15 \text{ m s}^{-1}$

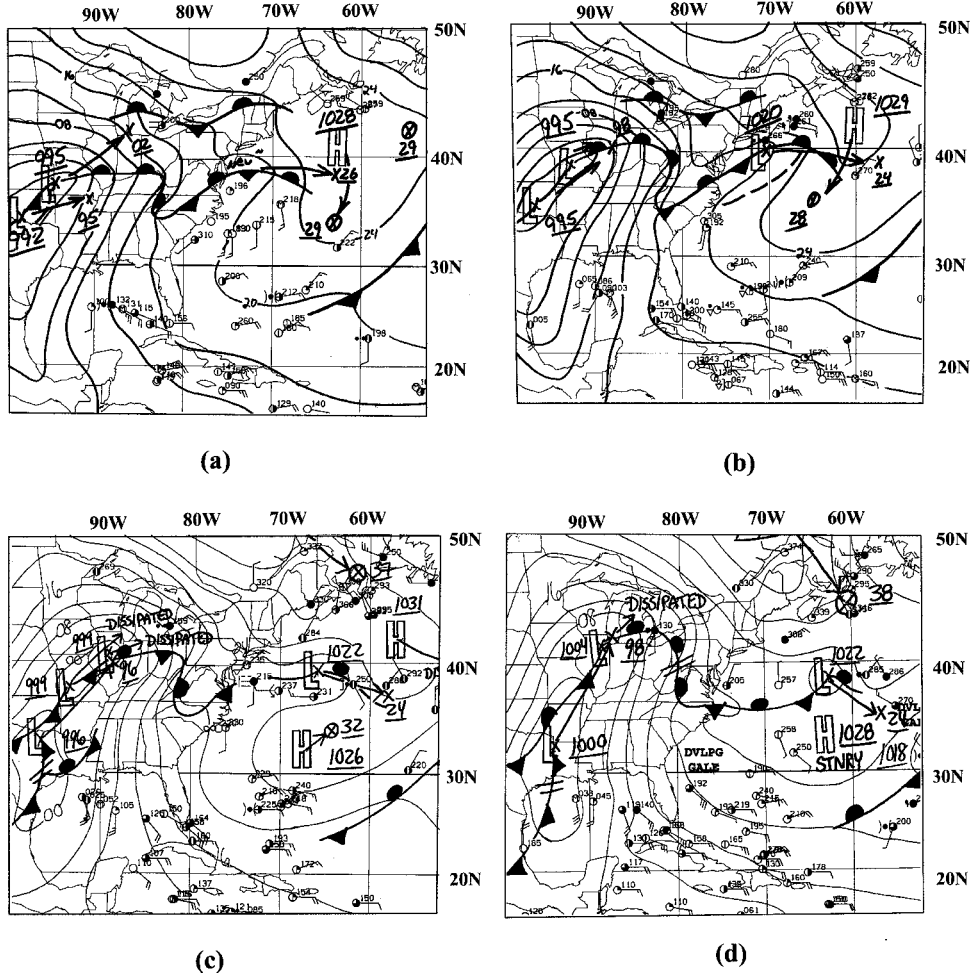


**Figure 3.** NOAA/National Weather Service (NWS)/NCEP surface analysis charts on January 22, 1999: (a) 0000, (b) 0600, (c) 1200, and (d) 1800 UT.

and a wind direction of  $319^\circ$  had been established and played a key role in generation of the observed waves. This surface wind vector is in good agreement with upper air radiosonde wind measurement below the inversion layer (i.e.,  $10.8 \text{ m s}^{-1}$  from  $300^\circ$  for the 970 to 850 mbar level).

### 3.2. Wave Forms

To better determine the nature of the observed waves, we will compare the observed wave forms with a theoretical model. *Zheng et al.* [1998a] developed a two-dimensional physical model and obtained an analytical form for the coastal lee wave solution. In their model, the  $x$  axis is perpendicular to the coastline, positive shoreward. The  $z$  axis is perpendicular to the sea surface, positive upward. The origin is located at the land

breeze front. The system is horizontally divided into two regions from the front at  $x = 0$ . The land breeze and vertical stratification occurs for  $x > 0$ . The model atmosphere has three layers. The upper layer has an infinite depth, while the lower layer, containing the land breeze, has a depth of  $H$ . There is a transition layer with a thickness of  $2\Delta H$  sandwiched between the two layers. The model may be considered to be a small-scale linear system. Then the wave equation and continuity equation are [Gossard and Hooke, 1975]

$$\frac{\partial^2 w}{\partial z^2} - k^2 w = 0 \quad (1)$$

$$\frac{\partial u}{\partial x} + \frac{\partial w}{\partial z} = 0, \quad (2)$$

where  $u$  and  $w$  represent the horizontal and vertical components of the wind velocity and  $k$  ( $= 2\pi/\lambda$ , where  $\lambda$  is the wavelength) represents the wavenumber. The amplitudes of the wind speeds in the two layers appear to be the same,  $u_0$ . Coastal lee wave can be expressed in the following form [Gossard, 1974]:

$$w = \frac{u_0 H \sinh(kz)}{L \sinh(kH)} \operatorname{sech}^2\left(\frac{x}{L}\right) \exp[i(kx - \sigma t)], \quad (3)$$

where  $L$  is the characteristic length of the frontal zone,  $\sigma$  is the angular frequency, and we take only the real part.

**Table 1.** Field Observation Instrument Locations and Elevations

Stations	Latitude	Longitude	Air Temperature Height, masl	Anemometer Height, masl
42020 Buoy	26°55'N	96°42'W	4	5
42035 Buoy	29°15'N	94°25'W	4	5
PTAT2 C-MAN	27°50'N	97°3'W	9.1	14.9
SRST2 C-MAN	29°40'N	94°3'W	12.8	13.4

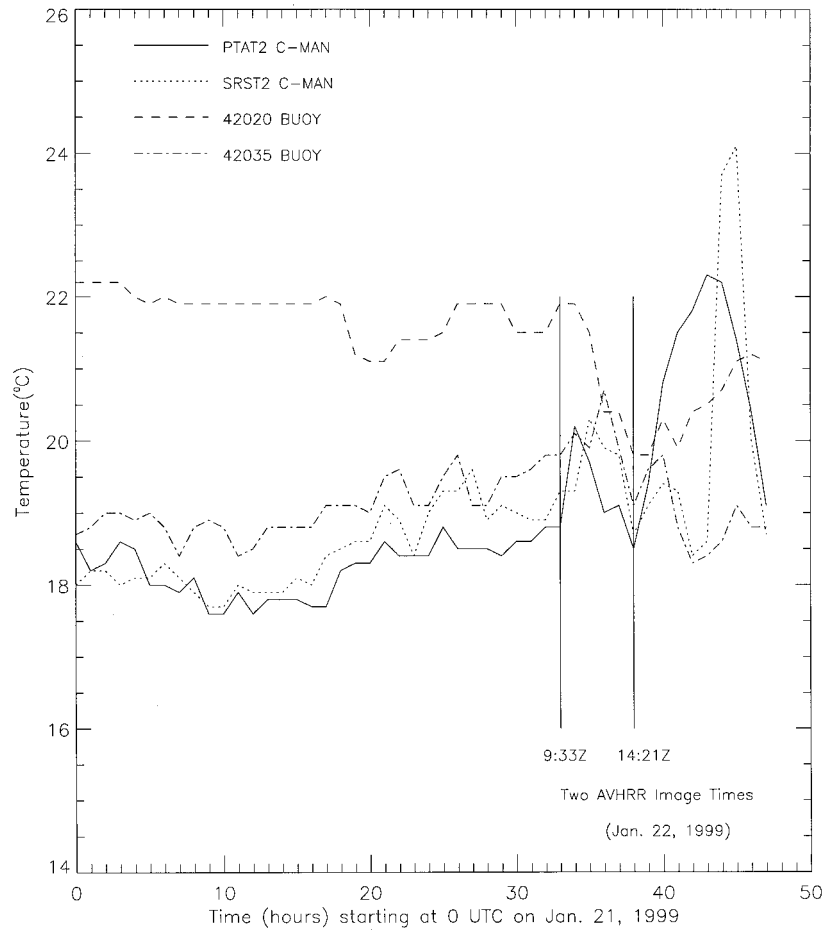


**Figure 4.** Hourly average sea surface air temperature measured at buoys 42020 (dashed line) and 42035 (dash dot line) and land surface air temperature measured at C-MAN stations PTAT2 (solid line) and SRST2 (dotted line).

The vertical amplitude of the wave,  $\eta$ , can be calculated from

$$\eta = \int_0^{T/4} w \, dt, \quad (4)$$

where  $T$  is the period of waves. Substituting (3) into (4) yields

$$\eta = \frac{u_0 H \sinh kz}{\sigma L \sinh kH} \operatorname{sech}^2\left(\frac{x}{L}\right) \exp[ikx], \quad (5)$$

where, again, only the real part is to be taken.

In this case the spatial characteristic scale of waves is  $L = O(10 \text{ km})$ , the characteristic velocity is  $U = O(15 \text{ m s}^{-1})$ , so that the Rossby number  $\varepsilon (= U/FL)$  is 15, which is much greater than 1. The motion is still at a small scale. Therefore the governing equations (4) and (5) are still valid. The wave amplitudes are related to the cloud top temperatures of the wave-like cloud patterns, which are measurable in the AVHRR IR images. Since the clouds are thick and opaque, the AVHRR channel 4 brightness temperature is essentially equal to the actual cloud top temperature [Mitchell *et al.*, 1990]. Therefore the pressure fields associated with the cloud top temperatures can be converted from the radiosonde measure-

ment. The results are plotted in Figure 6. We then converted the pressure field to altitude by using the hypsometric formula:

$$H = \frac{RT_0}{Mg} (\ln P_H - \ln P_0), \quad (6)$$

where  $H$  is the altitude above sea level in m,  $g$  is the gravitational acceleration  $9.8 \text{ m s}^{-2}$ ,  $M$  is the molecular weight of air  $28.9644 \text{ g mol}^{-1}$ ,  $R$  is the molar constant of gas  $8.3143 \text{ J mol}^{-1} \text{ K}^{-1}$ ,  $T_0$  is the virtual temperature in K, and  $P_H$  and  $P_0$  are the pressures in mbar at altitude  $H$  and at sea level, respectively. Comparisons of the model coastal lee wave (5) at  $z = H$ , with the wave forms derived from profiles A-A, B-B, and C-C in Figure 1a, are shown in Figure 7.

We see that the observed waves are reasonably well simulated by the theoretical model, especially for the first four leading waves. For the trailing waves the model provides an explanation for the amplitude decay but does not explain the shortening of wavelengths. This discrepancy likely reflects the nonlinear features of the observed waves, which cannot be described accurately with a linear wave model.

Since we cannot determine whether the temperature within the wave trough region (noncloudy band) was the atmosphere or the land surface, it is not feasible to estimate the wave

amplitude from the satellite images alone. In Figure 7, only the wave crests are plotted at their approximate altitude.

### 3.3. Dispersion Relation

The dispersion for the coastal lee waves can be derived from a quartic equation [Gossard and Hooke, 1975]:

$$\left(\frac{C}{u_0}\right)^4 - \left[1 + \frac{(2\alpha - 1)^2 - e^{-4\alpha}}{4\alpha^2} + \frac{R}{\alpha}\right] \left(\frac{C}{u_0}\right)^2 + \left(\frac{1 + R}{2\alpha} - 1\right)^2 - \left(\frac{1 + R}{2\alpha}\right)^2 e^{-4\alpha} = 0, \quad (7)$$

where  $C$  is the phase speed,  $\alpha = k\Delta H$ , and  $R (= \Delta\rho g\Delta H/\rho_0 u_0^2)$  is the Richardson number. In our case,  $\lambda = 9.5$  km,  $\Delta H$  is chosen as  $\lambda/2\pi$  ( $\approx 1.5$  km),  $\Delta\rho/\rho_0 = 0.013$ ,  $g = 9.8$  m s $^{-2}$ , and  $u_0 = 15$  m s $^{-1}$ . Thus there are two real solutions:

$$C_1 = 0.09u_0 \quad (8)$$

$$C_2 = 1.38u_0. \quad (9)$$

From (8) we conclude that the group speed is so small that we can consider that

$$C_g = 0. \quad (10)$$

This implies that the coastal lee waves may exist as stationary waves with respect to the atmospheric front. In an absolute reference frame that is fixed to the Earth's surface the wave velocity is

$$\mathbf{U} = \mathbf{U}_0 + \mathbf{C}, \quad (11)$$

where  $\mathbf{U}_0$  is the velocity of the moving reference frame. If  $\mathbf{U}_0 = U_0\mathbf{i}$ , for simplicity the group speed observed in the absolute system is

$$C_g = U_0. \quad (12)$$

This implies that the waves could move in step with the moving front. The behavior of the coastal lee wave packet is consistent with this. The surface observations and AVHRR images show that when the front moved seaward into the Gulf of Mexico, pushed from behind by the low-pressure system, the waves followed the front's movement. The second solution gives a large phase speed, which represents a fast propagating coastal lee wave. This solution, however, does not agree with our lee wave model. In our case the group speed cannot be estimated.

## 4. Conclusions and Discussion

Wave-like cloud patterns in NOAA AVHRR image taken over the Texas coastal region on January 22, 1999, were interpreted to be signatures of coastal lee waves, a type of small-scale atmospheric gravity wave. The waves occurred in the form of a wave packet containing 13 waves with an average wavelength of 9.5 km. The crest lines were generally parallel to the coastline with the crest length of the leading wave longer than 500 km. The life span of the event was estimated to have been of the order of 5 hours. Simultaneous field observations show that the sea surface air temperature was 2°–4°C higher than the land surface air temperature prior to the imaging time, constituting a favorable condition for driving a land breeze circulation. Time series of wind data measured at two C-MAN stations beneath the cloud patterns indicate a significant change in the wind speed and wind direction, implying that the land breeze circulation had been established simultaneously with the wave packet. The wave form of the observed waves is comparable with a theoretical model of the coastal lee waves.

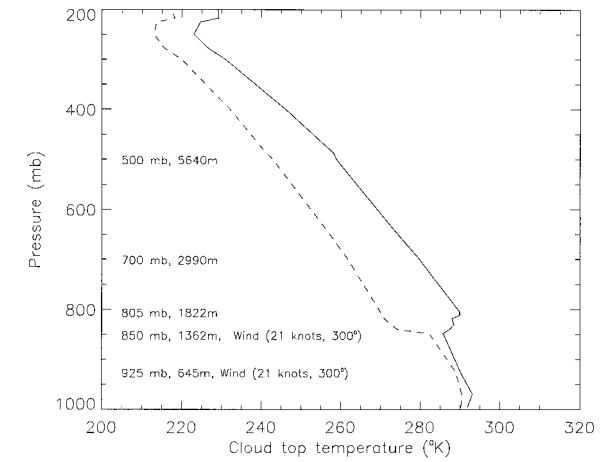


**Figure 6.** The virtual and dew point temperature profiles measured at nearest radiosonde station at Corpus Christi, Texas (27°34.8'N, 97°13.0'W) at 1200 UT on January 22, 1999. The wave shown in Figure 1a passed this station 3 hours prior to the radiosonde measurement.

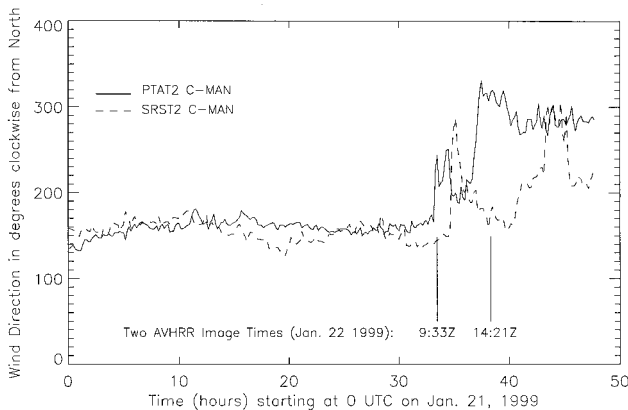
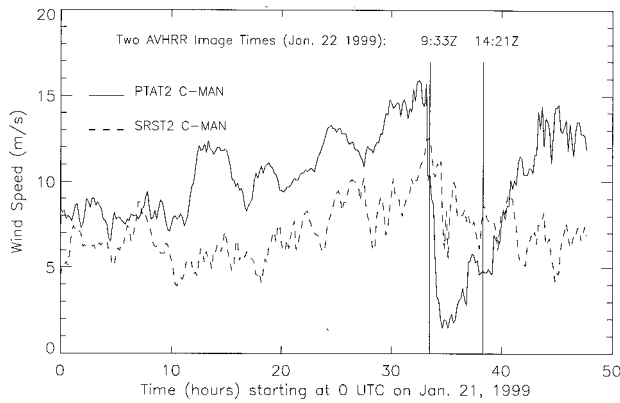


**Figure 5.** (a) Ten minute average wind speed and (b) wind direction time series measured at C-MAN stations PTAT2 (solid line) and SRST2 (dashed line).

From (3) we estimate that the vertical velocity of airflow

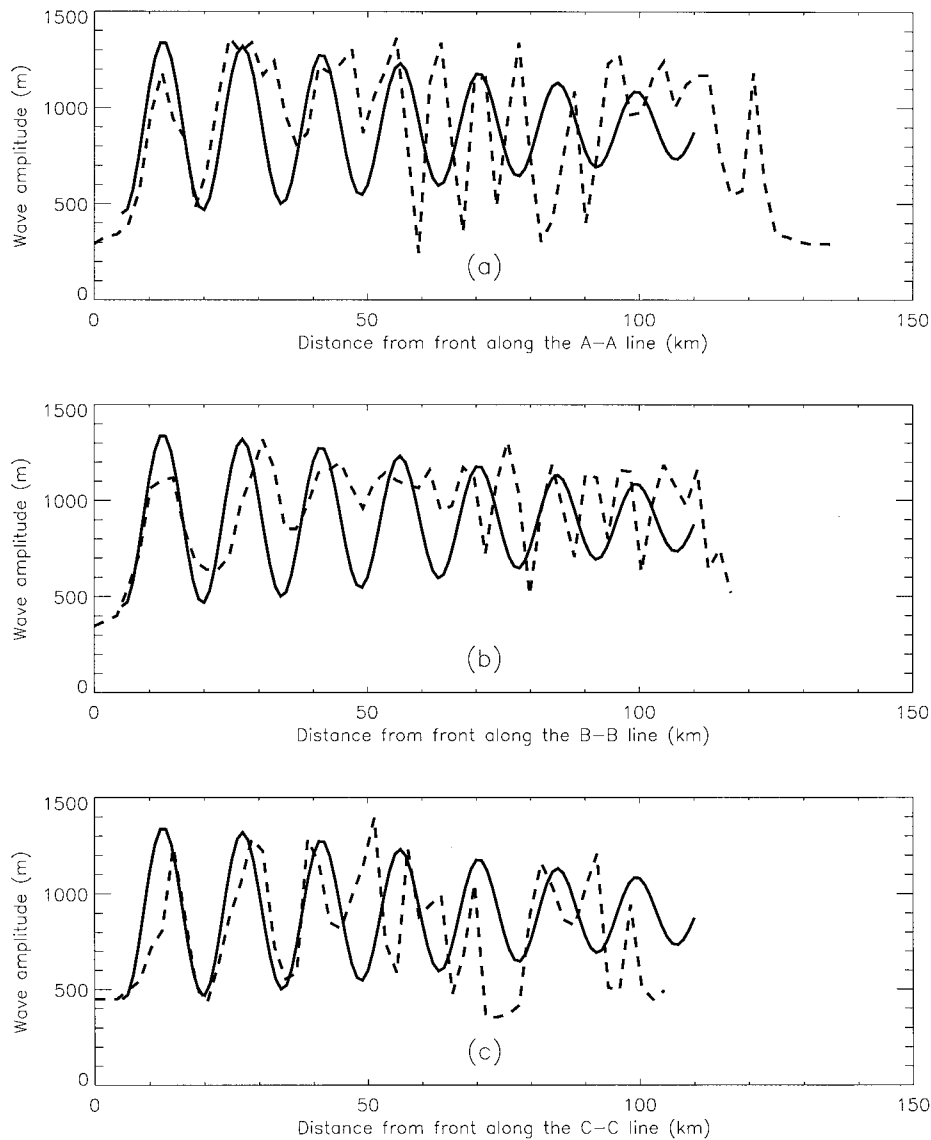


**Figure 7.** Comparisons of wave forms measured along lines (a) A-A, (b) B-B, and (c) C-C marked in Figure 1a with theoretical model of coastal lee waves.

induced by the coastal lee waves under investigation may reach  $0.3 \text{ m s}^{-1}$ . The amplitudes of the waves may reach 1 km as shown in Figure 7. This means that the waves may constitute a powerful disturbance for objects flying in the lower atmosphere, and some aircraft crashes happening along the coast may be related to this type of disturbance. The results of this study indicate that NOAA satellites are capable of providing visual and near real-time images of the waves, which can be used as a baseline for forecasting and research. On the basis of these results we conclude that the observed case provides new evidence for the occurrence of coastal lee waves along the U.S. coast. We also note the nonlinear features of the waves, which will be analyzed in future efforts.

**Acknowledgments.** This work was supported by the NOAA/NESDIS Ocean Remote Sensing Program and was partially supported by NASA NSCAT and EOS Interdisciplinary Science Investigations programs, the NASA JASON program through grant NAG5-7949, the NOAA Sea Grant Program through grant NA96RG0029, and NSF PFF OCE-9453499. We would like to thank Karen Friedman for help-

ing with the figures. The buoy and C-MAN station temperature and wind data were downloaded from NOAA's NDBC web site at <http://www.ndbc.noaa.gov>. Radiosonde data were downloaded from the University of Wyoming Atmosphere Science Department web site at <http://www.das.uwyo.edu/upperair>.

## References

- Clarke, R. H., The morning glory: An atmospheric hydraulic jump, *J. Appl. Meteorol.*, *11*, 304–311, 1972.
- Gjevik, B., and T. Marthinsen, Three-dimensional lee-waves pattern, *Q. J. R. Meteorol. Soc.*, *104*, 947–957, 1978.
- Gossard, E. E., Dynamic stability of an isentropic shear layer in a statically stable medium, *J. Atmos. Sci.*, *31*, 488–492, 1974.
- Gossard, E. E., and W. H. Hooke, *Waves in the Atmosphere*, 456 pp., Elsevier Sci., New York, 1975.
- Li, X., W. G. Pichel, K. S. Friedman, and P. Clemente-Colón, The sea surface imprint of island lee waves as observed by RADARSAT synthetic aperture radar, paper presented at IEEE International Geoscience and Remote Sensing Symposium, Inst. of Electr. and Electr. Eng., Seattle, Wash., 1998a.
- Li, X., W. Pichel, P. Clemente-Colón, V. Krasnopolsky, and J. Sapper, Validation of coastal sea and lake surface temperature measure-

- ments derived from NOAA/AVHRR data, paper presented at 5th International Conference on Remote Sensing for Marine and Coastal Environments, Environ. Res. Inst. of Mich., San Diego, Calif., 1998b.
- Mitchell, R. M., R. P. Cechet, P. J. Turner, and C. C. Elsum, Observation and interpretation of wave clouds over Macquarie Island, *Q. J. R. Meteorol. Soc.*, *116*, 741–752, 1990.
- Panchev, S., *Dynamic Meteorology*, 360 pp., D. Reidel, Norwell, Mass., 1985.
- Simpson, J. E., *Sea Breeze and Local Winds*, 234 pp., Cambridge Univ. Press, New York, 1994.
- Smith, R. K., Traveling waves and bores in the lower atmosphere: The “morning glory” and related phenomena, *Earth Sci. Rev.*, *25*, 267–290, 1988.
- Vachon, P. W., O. M. Johannessen, and J. A. Johannessen, An ERS-1 synthetic aperture radar image of atmospheric lee waves, *J. Geophys. Res.*, *99*, 22,483–22,490, 1994.
- Zheng, Q., X.-H. Yan, V. Klemas, C.-R. Ho, N.-J. Kuo, and Z. Wang, Coastal lee waves on ERS-1 SAR images, *J. Geophys. Res.*, *103*, 7979–7993, 1998a.
- Zheng, Q., X.-H. Yan, W. T. Liu, V. Klemas, D. Greger, and Z. Wang, A solitary wave packet in the atmosphere observed from space, *Geophys. Res. Lett.*, *25*, 3559–3562, 1998b.
- 
- P. Clemente-Colón, X. Li, and W. G. Pichel, NOAA/NESDIS, E/RA3, Room 102, WWBG, 5200 Auth Road, Camp Springs, MD 20746–4304. (xiaofeng.li@noaa.gov)
- W. T. Liu, Jet Propulsion Laboratory 300-323, California Institute of Technology, Pasadena, CA 91109.
- X.-H. Yan and Q. Zheng, College of Marine Studies, University of Delaware, Newark, DE 19716.

(Received June 21, 1999; revised June 29, 2000; accepted September 8, 2000.)

